The 8th European Congress on Computational Methods in Applied Sciences and Engineering
ECCOMAS Congress 2022
5-–9 June 2022, Oslo, Norway

SIMULATION OF SOFT ROBOTS WITH NONLINEAR MATERIAL BEHAVIOR USING THE COSSERAT ROD THEORY

Malte Grube[1] and Robert Seifried[1]

[1] Institute of Mechanics and Ocean Engineering
Hamburg University of Technology
Eissendorfer Strasse 42, 21073 Hamburg, Germany
e-mail: [malte.grube, robert.seifried]@tuhh.de, https://www.tuhh.de/mum/en/home.html

Key words: Soft Robotics, Cosserat Rod, Nonlinear Material

Abstract. For the simulation and model-based control of soft robots accurate models are required. In this contribution the simulation of a simple soft robot with the cosserat rod theory is examined for both linear and nonlinear material models. The soft robot is fabricated out of silicone. Thereby stiffness and damping properties are investigated. In addition to the achievable accuracy, the computation time is also examined.

1 INTRODUCTION

Soft material robots are an emerging and fast-growing field of research with potential application in various technical fields. These applications include, but are not limited to, medical applications, gripping applications and all sorts of human-machine-interaction. In contrast to conventional rigid robots usually soft robots are made out of soft materials, like silicone, and undergo large deformations. Therefore, besides new actuators and sensors also new modeling concepts are currently being developed for soft robots.

Many soft robots use the bending deformation of long slender rods to generate the necessary motion. For example, the fingers of a flexible hand can be modeled as such a deformable rod. Therefore, besides piecewise constant curvature models [1] various rod theories are very popular for modeling soft robots. Especially different forms of the Cosserat rod theory are widely used [1].

In this contribution a simple soft robot segment based on [3] is modeled with the geometrically exact rod theory in the form of [2]. While in [2] linear material is assumed, this model is extended here with a nonlinear material law to allow a more accurate modeling.

For practical applications besides the accuracy also the effort to determine the required material parameters of the simulation model for a real robot is of importance. Additionally, for model-based control the computation time is of great importance. Therefore, the different models are compared concerning the achievable accuracy, the required computation time and the effort to determine the required material parameters of the model for a physical robot.

2 SIMULATION MODEL

For the modeling of soft robots often the cosserat rod theory is used. This theory can describe the behaviour of long slender structures with a partial differential equation (PDE). This PDE

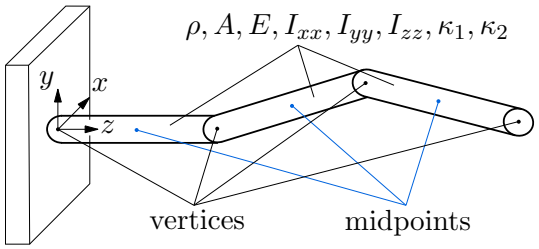

Figure 1: Schematic representation of a soft robot after discretization with the rod theory.

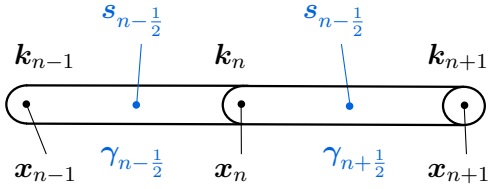

Figure 2: Location of the nodes in the rod theory. Black are position variables, blue are rotation variables.

usually has to be discretised to be solved. In this contribution, the geometrically exact rod theory in the form of [2] is used. The rod theory allows to model bending, torsion and elongation of a rod. The PDE is spatially discretized along the beam coordinate on a staggered grid as shown in fig. 1. The translatory degrees of freedom are located at the vertices, the rotatory degrees of freedom are located at the segment midpoints as quaternions. In the following, the index $n-\frac{1}{2}$ is used for quantities that are located on the midpoints between the nodes with the indices $n-1$ and n. This is shown in fig. 2. In this way, a set of ordinary differential equations is obtained.

For the calculation of the internal forces and torques bending, torsion, strain and shear of the rod have to be calculated. The curvature and torsion of two elements with respect to each other can be expressed by their quaternions $\boldsymbol{p}_{n-\frac{1}{2}}$ and $\boldsymbol{p}_{n+\frac{1}{2}}$. Here, the curvature is assigned to the translational node with index n. The vector of curvature and torsion $\boldsymbol{\kappa}_n$ is assigned to the vertices and can be calculated by

$$\boldsymbol{\kappa}_n = \frac{2}{\delta s_n} \xi(\theta_n) \cdot \mathfrak{I}(\boldsymbol{w}_n) \tag{1}$$

with

$$\boldsymbol{w}_n = \bar{\boldsymbol{p}}_{n-\frac{1}{2}} \cdot \boldsymbol{p}_{n+\frac{1}{2}}, \tag{2}$$

$$\theta_n = \arccos \mathfrak{R}(\boldsymbol{w}_n), \tag{3}$$

$$\delta s_n = \begin{cases} \frac{L}{2} & n = 0 \vee n = N \\ L. \end{cases} \tag{4}$$

Hereby $\xi(\theta_n)$ is a weighting function, $\bar{\boldsymbol{p}}_{n-\frac{1}{2}}$ describes conjugate quaternions, θ_n is the angle between $\boldsymbol{p}_{n-\frac{1}{2}}$ and $\boldsymbol{p}_{n+\frac{1}{2}}$ in the quaternionic space and L is the total length of the rod. In [2] different choices for the Weighting function $\xi(\theta_n)$ are discussed. One possible choice is

$$\xi(\theta_n) = \sqrt{\frac{2}{1+\cos\theta_n}}. \tag{5}$$

The vector of strain and shear $\boldsymbol{\gamma}$ of an element can be expressed as a function of the position of the end nodes $\boldsymbol{x}_n$ and $\boldsymbol{x}_{n-1}$. The vector of strain and shear $\boldsymbol{\gamma}$ is assigned to the midpoint of the element. For this holds

$$\boldsymbol{\gamma}_{n-\frac{1}{2}} = \boldsymbol{S}(\boldsymbol{p}_{n-\frac{1}{2}})^{\mathrm{T}} \cdot \frac{\boldsymbol{x}_n - \boldsymbol{x}_{n-1}}{L} - \begin{bmatrix} 0 & 0 & 1 \end{bmatrix}^{\mathrm{T}}. \tag{6}$$

Here $\boldsymbol{S}(\boldsymbol{p}_{n-\frac{1}{2}})$ is the rotation matrix to the quaternion $\boldsymbol{p}_{n-\frac{1}{2}}$. By total differentiation of the vector of curvature $\boldsymbol{\kappa}_n$ and the vector of strain and shear $\boldsymbol{\gamma}_n$ with respect to time, the rate of change of the curvature $\dot{\boldsymbol{\kappa}}_n$ and the rate of change of the strain and shear $\dot{\boldsymbol{\gamma}}_n$ needed for the damping terms are determined.

In the following, the index notation $n = 0, \ldots, N$ and $\nu = \frac{1}{2}, \ldots, N - \frac{1}{2}$ is used. The equation of motion can be derived to

$$\ddot{\boldsymbol{x}}_n = \frac{1}{\rho A \delta s_n} \left(\boldsymbol{p}_{n+\frac{1}{2}} \left(\boldsymbol{f}_{n+\frac{1}{2}} + \hat{\boldsymbol{f}}_{n+\frac{1}{2}} \right) \bar{\boldsymbol{p}}_{n+\frac{1}{2}} - \boldsymbol{p}_{n-\frac{1}{2}} \left(\boldsymbol{f}_{n-\frac{1}{2}} + \hat{\boldsymbol{f}}_{n-\frac{1}{2}} \right) \bar{\boldsymbol{p}}_{n-\frac{1}{2}} \right), \tag{7}$$

$$\ddot{\boldsymbol{p}}_\nu = \frac{2}{\rho L} \boldsymbol{\mu}(\boldsymbol{p}_\nu)^{\#} \left(4\rho \dot{\boldsymbol{p}}_\nu \boldsymbol{I} \dot{\bar{\boldsymbol{p}}}_\nu \boldsymbol{p}_\nu + \Delta \boldsymbol{x}_\nu \boldsymbol{p}_\nu \boldsymbol{f}_\nu + \boldsymbol{p}_{\nu+1} \boldsymbol{l}_{\nu+\frac{1}{2}} - \boldsymbol{p}_{\nu-1} \boldsymbol{l}_{\nu-\frac{1}{2}} + \boldsymbol{p}_\nu \hat{\boldsymbol{l}}_\nu \right) - |\dot{\boldsymbol{p}}_\nu|^2 \boldsymbol{p}_\nu \tag{8}$$

as described in [2]. In addition to the quantities already discussed, the density of the beam ρ, the rigid cross-sectional area A, the deformed length of the segment $\delta \boldsymbol{x}_\nu = \boldsymbol{x}_{\nu+\frac{1}{2}} - \boldsymbol{x}_{\nu-\frac{1}{2}}$, and the inertia matrix $\boldsymbol{I}$ occur. The latter is defined as

$$\boldsymbol{I} = \begin{pmatrix} 0 & & & \\ \hline & I_1 & & \\ & & I_2 & \\ & & & J \end{pmatrix}. \tag{9}$$

Here I_1 and I_2 are the second moments of area about the x- and y-axis, and J is the polar moment of inertia with respect to the z-axis. Furthermore, the internal forces $\boldsymbol{f}_{n+\frac{1}{2}}$ and internal torques $\boldsymbol{l}_\nu$ as well as the external forces $\hat{\boldsymbol{f}}_{n+\frac{1}{2}}$ and external torques $\hat{\boldsymbol{l}}_\nu$ occur. The expression $\boldsymbol{\mu}(\boldsymbol{p}_\nu)^{\#}$ is the pseudoinverse of the inertia matrix defined by [2]. When calculating the equations of motion, it is important to keep in mind that all products are quaternion products.

3 MATERIAL MODELS

In the equation of motion, the internal forces $\boldsymbol{f}_{n-\frac{1}{2}} = \boldsymbol{f}_{n-\frac{1}{2}}(t, \boldsymbol{x}, \boldsymbol{p}, \boldsymbol{\gamma}_{n-\frac{1}{2}}, \dot{\boldsymbol{\gamma}}_{n-\frac{1}{2}})$ and torques $\boldsymbol{l}_n = \boldsymbol{l}_n(t, \boldsymbol{x}, \boldsymbol{p}, \boldsymbol{\kappa}_n, \dot{\boldsymbol{\kappa}}_n)$ represent the material properties of the soft robot. In this contribution a linear viscoelastic material model and the Saint Venant–Kirchhoff material model are examined. These are briefly summarised in the following.

3.1 Linear material model

One of the simplest choices is to assume linear viscoelastic material behaviour. The internal forces and torques acting on the node with the index n respectively $n - \frac{1}{2}$ then result in

$$\boldsymbol{l}_n = \boldsymbol{C}^{\mathrm{K}} \boldsymbol{\kappa}_n + 2 \cdot \boldsymbol{C}^{\dot{\mathrm{K}}} \dot{\boldsymbol{\kappa}}_n, \tag{10}$$

$$\boldsymbol{f}_{n-\frac{1}{2}} = \boldsymbol{C}^{\gamma} \boldsymbol{\Gamma}_{n-\frac{1}{2}} + 2 \cdot \boldsymbol{C}^{\dot{\gamma}} \dot{\boldsymbol{\Gamma}}_{n-\frac{1}{2}} \tag{11}$$

with the stiffness matrices

$$\boldsymbol{C}^K = \begin{pmatrix} 0 & & & \\ \hline & EI_1 & & \\ & & EI_2 & \\ & & & GJ \end{pmatrix}, \tag{12}$$

$$\boldsymbol{C}^\gamma = \begin{pmatrix} 0 & & & \\ \hline & GA\kappa_1 & & \\ & & GA\kappa_2 & \\ & & & EA \end{pmatrix}. \tag{13}$$

The parameters of the stiffness matrices are the Young's modulus E, the shear modulus G, the second moments of area about the corresponding axes I_1 and I_2, the polar second moment of area J, the rigid cross-sectional area A and the shear correction factors κ_1 and κ_2.

The damping matrices

$$\boldsymbol{C}^{\dot{K}} = \left(\begin{array}{c|ccc} 0 & & & \\ \hline & c_1^{\dot{K}} & & \\ & & c_2^{\dot{K}} & \\ & & & c_2^{\dot{K}} \end{array}\right), \qquad (14) \qquad \boldsymbol{C}^{\dot{\gamma}} = \left(\begin{array}{c|ccc} 0 & & & \\ \hline & c_1^{\dot{\gamma}} & & \\ & & c_2^{\dot{\gamma}} & \\ & & & c_2^{\dot{\gamma}} \end{array}\right) \qquad (15)$$

can only be obtained experimentally. For simplicity a diagonal matrix structure is assumed. However, the generalisation to a non-diagonal structure is straightforward. As bending is by far the most important deformation and especially the elongation mode is rather stiff, in many applications it is sufficient to only determine the damping coefficients directly related to bending. The other damping coefficients should then be chosen sufficiently large to obtain good numerical properties.

3.2 Saint Venant–Kirchhoff material model

The Saint Venant–Kirchhoff material model is a nonlinear extension of Hooke's law. This allows to model larger deformations more accurately. The strain energy function of the Saint Venant–Kirchhoff model can be written as

$$\Psi_{\text{SV-Kirchhoff}} = \frac{1}{2}(\lambda + 2\mu) I_{E1}^2 - 2\mu I_{E2}. \qquad (16)$$

with the Lamé-constants μ and λ and the principal invariants I_{E1} and I_{E2} of the Green-Lagrange strain tensor $\boldsymbol{E}$ where $I_{E1} = \operatorname{Tr}(\boldsymbol{E})$ and $I_{E2} = \frac{1}{2}\left(\operatorname{Tr}(\boldsymbol{E})^2 - \operatorname{Tr}(\boldsymbol{E^2})\right)$ [6]. The second Piola-Kirchhoff strain tensor $\boldsymbol{S}$ can be calculated by partially differentiating the distortion energy Ψ with respect to the Green-Lagrange distortion tensor $\boldsymbol{E}$ and is given by

$$\boldsymbol{S} = \lambda I_{E1} \cdot \boldsymbol{I} + 2\mu \boldsymbol{E}. \qquad (17)$$

The relation between $\boldsymbol{S}$ and $\boldsymbol{E}$ is materially linear, but geometrically nonlinear. The geometric nonlinearity results from the geometric nonlinearity of the strain tensor $\boldsymbol{E}$ and the second Piola-Kirchoff stresses $\boldsymbol{S}$. In this context, it should be noted that although Saint-Venant-Kirchhoff's law can describe large deformations, it only applies in the case of small distortions. This is often the case in the application of soft robots, since for geometric reasons, they usually have a significantly higher stiffness against deformation than against bending and torsion [2]. The internal forces and torques can then be derived from the strain energy function $\Psi_{\text{SV-Kirchhoff}}$ in eq. (16) as described in [7]. Compared to the linear material model three instead of only two material parameter have to be determined. This can usually only be done experimentally.

3.3 Determination of stiffness parameters

A key challenge, which often dominates the effort to set up the simulation model of a real robot, is to determine the material parameters. To reduce the effort, it is important to keep the number of parameters to be determined experimentally as low as possible. For the stiffness matrices $\boldsymbol{C}^K$ and $\boldsymbol{C}^\gamma$ the geometric parameters A_1, A_2, A, I_1, I_2, J, κ_1, κ_2 and the material

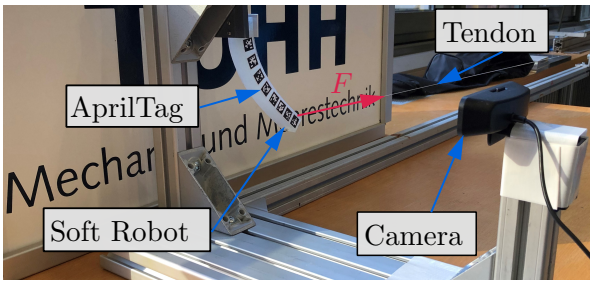

Figure 3: Experimental setup.

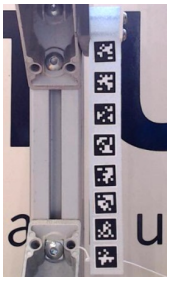

Figure 4: Rod with AprilTags.

parameters G and E have to be determined. The shear correction factors κ_1 and κ_2 should not be confused with the vector of curvature and torsion $\boldsymbol{\kappa}_n$. The geometric parameters can usually be measured directly.

The determination of the material parameters is more challenging. The only known material parameters for silicone are usually the shore Hardness H, which is often given by the manufacturer in the datasheet, and the poisson's ratio ν, which is approximately $\nu \approx 0.5$ as silicone is nearly incompressible. The Young's modulus E cannot be determined exactly from the shore hardness H. However, there are different approximation formulas to determine the Young's modulus E from the shore hardness H [5]. One of the most widely used formulas to obtain the Young's modulus from the shore-A hardness is the semi-empirical equation by [4]

$$E = \frac{0.0981 \cdot (56 + 7.62336 \cdot H)}{0.137505 \cdot (254 - 2.54 \cdot H)} \tag{18}$$

with the Young's modulus E then given in MPa. The shear modulus G can then be easily calculated to

$$G = \frac{E}{2 \cdot (1 + \nu)}. \tag{19}$$

For comparison, in a second simulation an experimentally determined value for the Young's modulus is used. It is determined from the experiments described in section 4 in such a way that the error of the simulation is minimized compared to the experiment. For the Saint Venant–Kirchhoff material model all material parameters are fitted to the experimental data.

4 EXPERIMENTAL SETUP

For the experimental evaluation of the simulation model, a silicone rod with a length of $L = 125\,\mathrm{mm}$, a cross section of $A = 20 \times 20\,\mathrm{mm}^2$ and a shore hardness of $H = 43\,\mathrm{SHORE\,A}$ is examined in experiments and simulations. These dimensions are typical for many soft robotic applications. The experimental setup is shown in fig. 3 and fig. 4. The rod is clamped at one end, so that the longitudinal axis of the rod is orientated vertically. At the other end a horizontal force F is applied via a tendon. For the measurement of the deformation eight AprilTag markers are fastened at the rod, which are tracked with a camera. For each of the markers, the position and orientation in space (6 DOF) can be determined from the camera image.

The simulation model of the rod is evaluated with two different experiments. For the examination of the stiffness properties different forces F up to $3\,\mathrm{N}$ are applied to the rod, both

in experiments and simulations, in a first step the steady state bending line is considered. The maximum force F is chosen such that a typical maximum deformation of a soft robot, like e.g. of a soft gripper, is represented. In a second setup the dynamic damping properties are examined. Therefore, the beam is deflected and then released from this position. Thereby, the deflection of the beam is observed over time.

5 EXPERIMENTAL RESULTS

The results of the experiments described in section 4 are evaluated for the stiffness and the damping properties in the following. The computation time for the simulation with the linear material model and the Saint Venant-Kirchhoff material model are almost the same. The simulation of a 5 s long damped oscillation of the rod takes approximately 1.7 s and is therefore real-time capable.

5.1 Stiffness

In fig. 5 the bending line of the silicone beam is shown for different static loads F, both for simulations and the experiments. For the simulations linear material models are used with the Young's modulus E calculated with eq. (18). A good agreement of the shape of the deformation can be seen, however, the deflection in the experiment is about 20 % larger than in the simulation. This can be explained by an inaccurate approximation of the Young's modulus. An improvement of the simulation accuracy could be archived by fitting the Young's modulus E to the experimental data. The results are shown in fig. 6. With the fitted values a very good agreement of the simulation and the experiment can be observed.

The results for the simulation with the Saint Venant–Kirchhoff model are shown in fig. 7. As with the linear material models with fitted Young's modulus a good agreement between experiment and simulation can be observed. In fig. 8 the absolute and the relative error of the tip position of the silicone beam are shown for different forces F for both, the linear model with fitted Young's modulus and the Saint Venant–Kirchhoff model. Overall the error of the Saint Venant–Kirchhoff model is a bit lower than for the linear material model. Only for very small deflections a slightly larger error of the Saint Venant–Kirchhoff model could be observed.

The reason for the comparatively good simulation results with the linear material models is that the experiments were mainly performed in the linear range of the material behaviour of the silicone. It can be expected that the simulation results for much larger deflections of the silicone rod will show a larger simulation error. However, in practical applications such large deflections are often not reached as very high forces are needed which are difficult to apply to a soft robot and might lead to material damage.

5.2 Damping

In fig. 9 and fig. 10 the deflection of the beam is plotted over time together with a least-squares fit of an exponential envelope. In general, systems with linear damping properties have an exponential envelope. It can be seen that the exponential envelope is not a good fit for the oscillations with large amplitude in the first 1 s. However, for smaller deflections starting at 1.5 s a very good fit can be archived with the exponential envelope. This can be explained by linear damping properties for oscillations with low amplitude as also included in the model. In

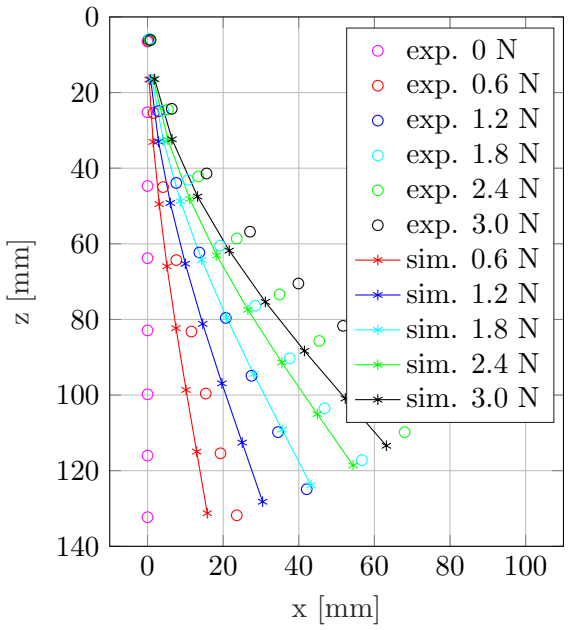

Figure 5: Bending line in simulation and experiment with linear material laws and approximated Young's modulus.

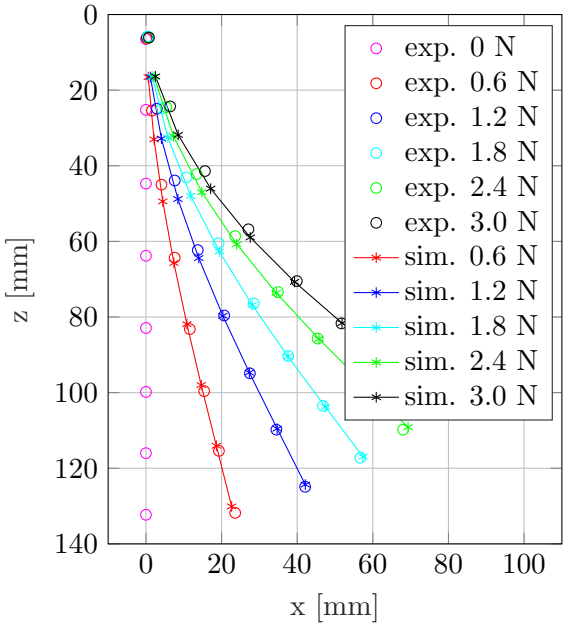

Figure 6: Bending line in simulation and experiment with linear material laws and fitted young's modulus.

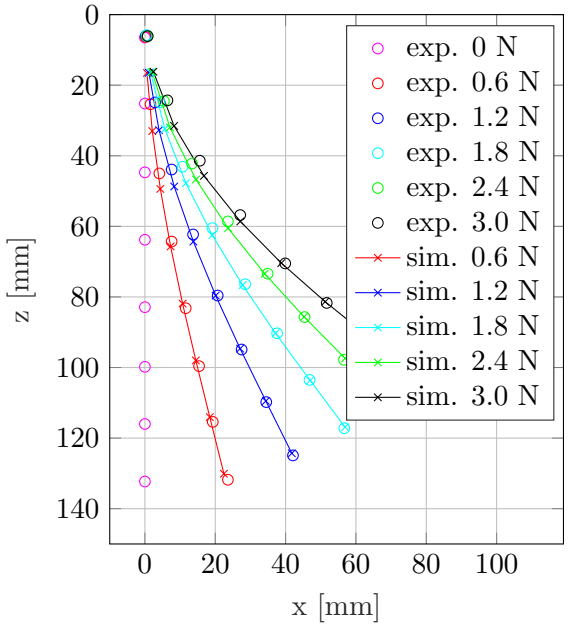

Figure 7: Bending line in simulation and experiment with the Saint Venant–Kirchhoff material laws and fitted Young's modulus.

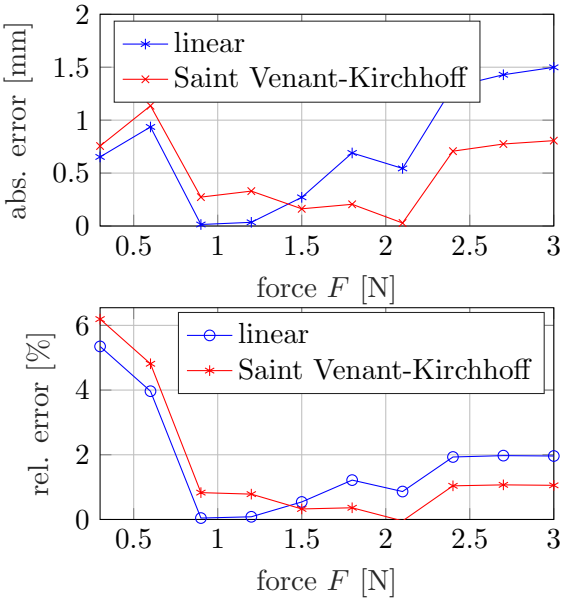

Figure 8: Absolute and relative position error of the endpoint for the linear and the Saint Venant–Kirchhoff material model.

contrast nonlinear damping properties for oscillations with larger amplitudes occur, which is not included in the model. As oscillations with high amplitudes are usually not desirable and should be avoided for most practical applications a linear damping model is sufficient.

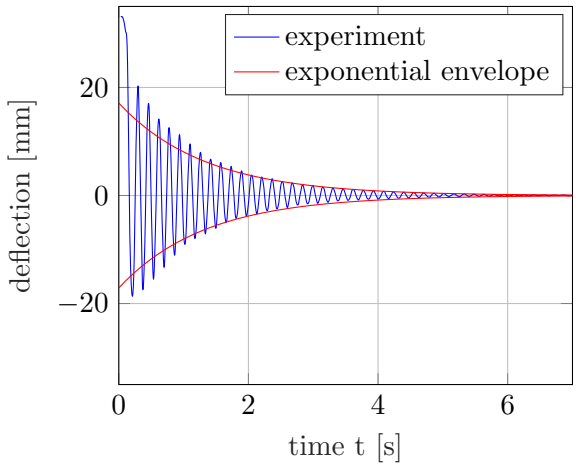

Figure 9: Damping behaviour of the silicone rod with fitted exponential envelope.

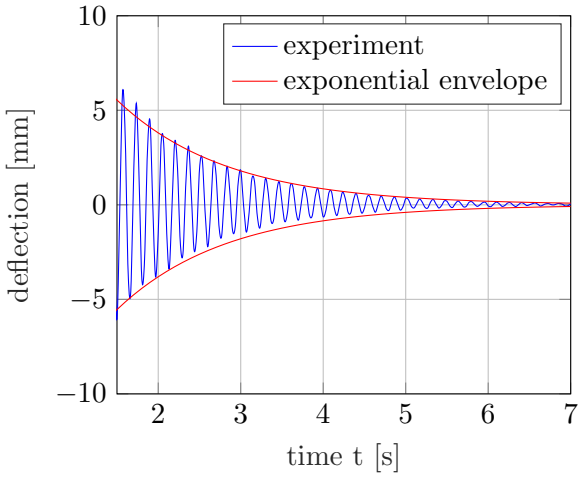

Figure 10: Damping behaviour of the silicone rod for small amplitudes with fitted exponential envelope.

6 CONCLUSIONS

In this contribution the simulation of a simple rod-shaped soft robot out of silicone was examined experimentally for both, a linear and a nonlinear material model. Already with the linear material model very good simulation results could be obtained, if the Young's modulus is determined from experiments. This is probably sufficient for most soft robot applications. The use of nonlinear material models could only slightly improve the simulation results.

For the linear material laws, all required material parameters could be determined approximately from the data sheet information of the silicone used. For the nonlinear material model used, this is no longer possible since an additional material parameter is required. However, it may also be useful for the linear material model to determine the material parameters experimentally in order to increase the accuracy. In the example considered in this paper, the calculated value for the modulus of elasticity was 20 % greater than the experimentally determined value.

The examination of the damping behaviour showed, that for oscillations with small and medium amplitude linear viscous damping can be assumed. Only for oscillations with higher amplitude nonlinear effects have to be considered. Because large oscillations are usually not desirable for many practical applications linear damping models are sufficient.

REFERENCES

[1] C. Lee, M. Kim, Y. J. Kim, N. Hong, S. Ryu, H. J. Kim, and S. Kim, Soft Material Robot Review. *IJCAS*, Vol. **15**, pp. 3-15, 2017

[2] H. Lang, J. Linn and M. Arnold, Multi-body dynamics simulation of geometrically exact Cosserat rods. *Multibody Syst Dyn.*, Vol. **25**, pp. 285–312, 2011.

[3] M. Grube and R. Seifried, Curvature Sensing of a Soft Robot based on Conductive Foam. *Proceedings in applied mathematics and mechanics*, Vol. **21**, 2021.

[4] A. N. Gent, On the Relation between Indentation Hardness and Young's Modulus. *Rubber Chemistry and Technology*, Vol. **31**, pp. 896–906, 1958.

[5] Kent Larson, Can you estimate modulus from durometer hardness for silicones. *Dow Corning Corporation*, 2016.

[6] E.W.V. Chaves, *Notes on Continuum Mechanics.* Dordrecht: Springer Netherlands, 2013.

[7] J.C. Simo, A Finite Strain Beam Formulation. The Three-Dimensional Dynamic Problem. Part I. *Computer Methods in Applied Mechanics and Engineering*, Vol. **49**, pp. 55–70, 1985